

Critical Oxide Thickness for Efficient Single-walled Carbon Nanotube Growth on Silicon Using Thin SiO₂ Diffusion Barriers

J. M. Simmons,¹ Beth M. Nichols,² Matthew S. Marcus,^{1,2}

O. M. Castellini,¹ R. J. Hamers,² and M. A. Eriksson¹

¹*Department of Physics, University of Wisconsin - Madison*

²*Department of Chemistry, University of Wisconsin - Madison*

Abstract

The ability to integrate carbon nanotubes, especially single-walled carbon nanotubes, seamlessly onto silicon would expand the range of applications considerably. Though direct integration using chemical vapor deposition is the simplest method, the growth of single-walled carbon nanotubes on bare silicon and on ultra-thin oxides is greatly inhibited due to the formation of a non-catalytic silicide. Using x-ray photoelectron spectroscopy, we show that silicide formation occurs on ultra-thin oxides due to thermally activated metal diffusion through the oxide. Silicides affect the growth of single-walled nanotubes more than multi-walled nanotubes due to the increased kinetics at the higher single-walled nanotube growth temperature. We demonstrate that nickel and iron catalysts, when deposited on clean silicon or ultra-thin silicon dioxide layers, begin to form silicides at relatively low temperatures, and that by 900 °C, all of the catalyst has been incorporated into the silicide, rendering it inactive for subsequent single-walled nanotube growth. We further show that a 4 nm silicon dioxide layer is the minimum diffusion barrier thickness which allows for efficient single-walled nanotube growth.

Keywords: Carbon nanotubes, Catalysis, Chemical vapor deposition, Photoelectron spectroscopy

Corresponding author:

M. A. Eriksson

Department of Physics, University of Wisconsin - Madison

1150 University Ave.

Madison, WI 53706

e-mail: maeriksson@wisc.edu

I. INTRODUCTION

Since their discovery, carbon nanotubes have shown great promise for a wide variety of applications which utilize their unique electronic and mechanical properties.^[1] For applications in which individual nanotubes act as the working element, such as nanotube field effect transistors (FETs)^[2,3] or chemical sensors,^[4,5,6] it is important to control the location and orientation of the nanotubes. Nanotubes can be prefabricated and then assembled into the desired geometry, or they can be fabricated in place using chemical vapor deposition (CVD).^[7,8] CVD is preferred since the growth can be widely tuned, both in yield and structure (single- vs. multi-walled), by modifying the experimental conditions. While there are a vast number of CVD recipes available in the literature for both single- and multi-walled nanotube growth, most studies of the growth process have focused on the role of the carbon precursor (e.g. CO, CH₄, C₂H₂) and temperature as control parameters with less attention placed on the choice of catalyst and substrate.^[9] Optimization of the catalytic process requires an understanding of the catalyst chemistry throughout the growth process, including the initial chemical state of the catalyst before the introduction of the feedstock, as well as the catalytic decomposition of the feedstock in or on the catalyst particle.^[10,11,12,13,14,15,16] Only recently have studies focused on the catalyst-feedstock and catalyst-substrate interaction.^[14,15,16,17,18,19,20]

It is well established that the yield of single-walled nanotube growth on silicon substrates is dramatically reduced compared with growth on thick silicon dioxide layers, due to poisoning of the catalyst by the formation of a silicide.^[12,21,22,23] Intriguingly, the growth of multi-walled nanotubes on silicon substrates is regularly reported and seems less susceptible to catalyst poisoning,^[24,25,26,27] yet the cause of this difference has not been addressed. For device applications it is desirable to use thin oxides to increase the gate capacitance and gate efficiency, and thus it is important to understand how to minimize oxide thickness while still preventing catalyst poisoning. Though thick silicon dioxide layers have been used as diffusion barriers during nanotube growth, there has been no investigations to date that determine the effectiveness of ultra-thin oxides.

Here we demonstrate explicitly that catalyst diffusion through the ultra-thin silicon dioxide layer controls the formation of the non-catalytic silicide. Using x-ray photoelectron spectroscopy (XPS), we study the interfacial reactions between the substrate and iron-

or nickel-based nanotube catalysts during the initial temperature ramp portion of a CVD growth cycle. We show that ultra-thin oxide layers (4 nm or greater) are sufficient to inhibit the silicide formation and permit high yield growth of single-walled carbon nanotubes. On thinner oxides or clean silicon, silicide formation begins by 600 °C (Ni) or 800 °C (Fe) and the catalyst is entirely consumed in the silicide at the growth temperature of single-walled nanotubes. The silicide formation temperatures account for the difference in single- versus multi-walled nanotube growth because multi-walled nanotubes are grown at lower temperatures where some of the catalyst remains unreacted and active for catalysis. Interestingly, the silicides form while the silicon dioxide is still present on the substrate, indicating that diffusion of metal or silicon through the oxide is occurring. We show that it is metal diffusion through the oxide, forming a metal silicide underneath the oxide, which dominates the interfacial reactions between the nanotube catalyst and the silicon substrate.

II. RESULTS AND DISCUSSION

To understand the catalyst-substrate interfacial reactions, we first analyze XPS spectra of iron nitrate catalyst that has been deposited on a thick (100 nm) thermal oxide. On thick oxides, silicides will not form and single-walled nanotube growth occurs with high yield (Figure 1a). Before annealing, the iron core level (Figure 1b) exhibits broad, asymmetric peaks at 710.8 eV and 724.5 eV, corresponding to the Fe 2p_{3/2} and 2p_{1/2} levels of iron oxide in a mixed Fe²⁺/Fe³⁺ oxidation state.^[28,29] The extra intensity on the high binding energy side of the core levels is due to unresolved satellites that are characteristic of oxidized iron.^[29,30] As the catalyst is heated on the thick oxide, there are no major changes in the chemistry of the iron oxide. There is a small loss in iron intensity, due to either agglomeration of the catalyst on the surface (thereby reducing the measured intensity due to the finite electron escape depth) or desorption of the iron into the vacuum while annealing.^[13] There is also a shift in the center of gravity of the Fe 2p_{3/2} core level as the Fe²⁺ oxide (FeO) transforms into the more stable Fe³⁺ oxide (Fe₂O₃)^[31] and the satellite peaks at 715 eV and 730 eV become better defined. Even at 1000 °C, the catalyst remains as iron oxide because there is no reaction pathway to reduce it to pure iron. The necessary reduction to metallic iron in a CVD reactor would come from flowing hydrogen or from feedstock decomposition products, enabling the catalysis of carbon nanotube growth.

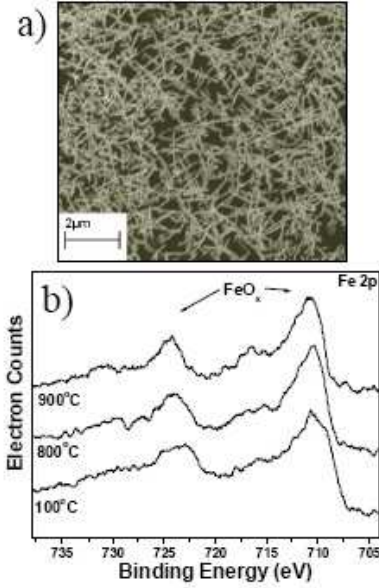


FIG. 1: (a) SEM image of high-yield nanotube growth on 100 nm SiO₂. (b) Fe 2p core level spectra of iron nitrate catalyst on 100 nm SiO₂. As the sample is annealed, there is no appreciable change in the oxidation state of the iron.

At the opposite extreme - that of hydrogen-terminated silicon on which single-walled nanotube growth is inhibited - surface reactions play a major role in the evolution of catalyst chemistry even at low temperatures. While iron nitrate catalyst that has been deposited on a hydrogen terminated silicon substrate remains oxidized at room temperature (Figure 2b), the center of gravity of the Fe 2p_{3/2} core level is shifted to 710.5 eV, indicating that the iron has been partially reduced as compared to the catalyst on the thick oxide. Whereas the Si 2p spectrum of the thick oxide shows only a peak at 103.3 eV due to the SiO₂ layer, the spectrum of the hydrogen-terminated substrate (Figure 2a) at room temperature resolves the Si 2p atomic core levels (99.3 and 103.3 eV), as well as a small, broad peak on the high binding energy side of the Si 2p peak, at around 102.7 eV, indicating the formation of a non-stoichiometric silicon suboxide.^[32] This suboxide could have formed in air after the HF oxide strip but before introduction in the vacuum chamber, or could account for the small amount of reduction in the iron as compared with the catalyst on the thick oxide. Reports have indicated that a silicon dioxide is more stable than either FeO or Fe₂O₃, which could lead to an exchange of oxygen from the iron oxide to the silicon substrate,^[31,33] even at low temperature.

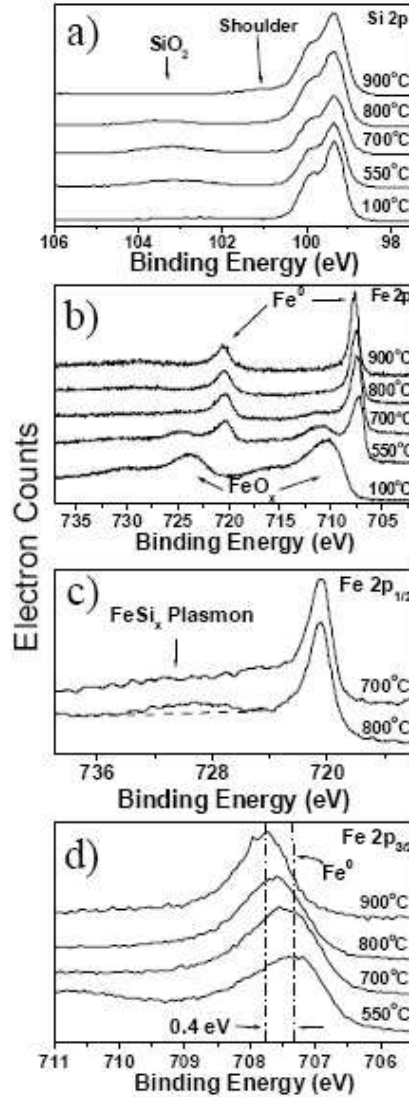


FIG. 2: XPS spectra of iron nitrate on clean silicon, for the (a) Si 2p and (b) Fe 2p core levels. At low annealing temperatures, the iron is reduced by the silicon substrate, forming a thin layer of SiO₂. By 800 °C, the iron begins to alloy with the substrate, forming an iron silicide, seen in (d) by a 0.4 eV shift in the Fe 2p_{3/2} core level and in (c) by the emergence of a plasmon loss peak.

In contrast to the thick oxide, iron catalyst deposited on hydrogen terminated silicon begins to reduce to metallic iron when the catalyst by the time it is annealed to 550 °C. This is seen in figure 2b by the decrease in Fe 2p intensity at 710.5 eV, 724.1 eV, and the associated satellites of iron oxide, and by the appearance of peaks at 707.4 eV and 720.7 eV corresponding to the Fe 2p core levels of Fe⁰. The iron oxide is further reduced as the substrate is annealed, indicated by the reduced intensity of the iron oxide peaks

(Figure 2b). By 800 °C, the iron oxide has been fully reduced. As in the case of a thick oxide, the reduction in UHV must come from a surface reaction between the oxidized catalyst and the substrate. Indeed, there is an appreciable exchange of oxygen from the iron oxide to the silicon substrate, leading to a marked increase in intensity of the silicon oxide peak, accompanied by a shift in the peak position to higher binding energies (Figure 2a). At 550 °C the silicon oxide peak shifts to higher binding energy, and between 700 °C and 800 °C the peak reaches 103.3 eV which is characteristic of stoichiometric SiO₂. This indicates that the iron oxide catalyst is reduced by the silicon substrate leading to the formation of a thin SiO₂ layer.

After the iron has been fully reduced at 800 °C, the catalyst begins to form a silicide. At 800 °C, the Fe 2p_{3/2} core level has shifted to higher binding energy by approximately 0.2 eV (Figure 2d), and a very broad peak begins to appear in the Fe 2p spectrum centered around 729 eV (Figure 2c). In the silicon core levels, a small shoulder appears at 100.5 eV on the high binding energy side of the Si 2p peak (Figure 2a). By 900 °C, the Fe 2p_{3/2} peak has shifted further to 707.8 eV, giving a total binding energy increase of 0.4 eV (Figure 2d). The 0.4 eV total shift in the Fe 2p_{3/2} peak position, accompanied by the appearance of a peak ~21 eV higher in binding energy, is indicative of the formation of an iron silicide, likely FeSi₂.^[34] The peak at 729 eV is due to a plasmon loss, seen in Figure 2c, and has been observed in electron energy loss spectroscopy^[35] as well as XPS^[12,34] investigations of Fe/Si multilayers. Further, the intensity of the shoulder on the Si 2p peak increases and the SiO₂ has desorbed entirely as evidenced by the loss of the ~103.3 eV feature in the Si 2p spectrum. Though the shoulder in the Si 2p spectrum at 100.5 eV seems to be associated with the formation of the silicide, the apparent binding energy of the shoulder is too high to be due to a FeSi_x core level which would be expected to be shifted by only ~0.2 eV.^[34] At present, the origin of this shoulder is not known. Annealing at 1000 °C (not shown) only leads to a decrease in the intensity of the iron peaks, but causes no noticeable changes in the peak positions, indicating that the silicide formation is complete at 900 °C.

Catalyst poisoning by silicide formation is not unique to iron. New also see that nickel thin film catalyst on clean silicon is incorporated into a silicide, only at a much lower temperature. Whereas iron catalyst is not fully reduced until 800 °C, the native nickel oxide has been fully reduced by 600 °C, and is accompanied by the growth of a SiO₂ layer (Figure 3a,b). By 600 °C some of the nickel has also been incorporated into a silicide, seen

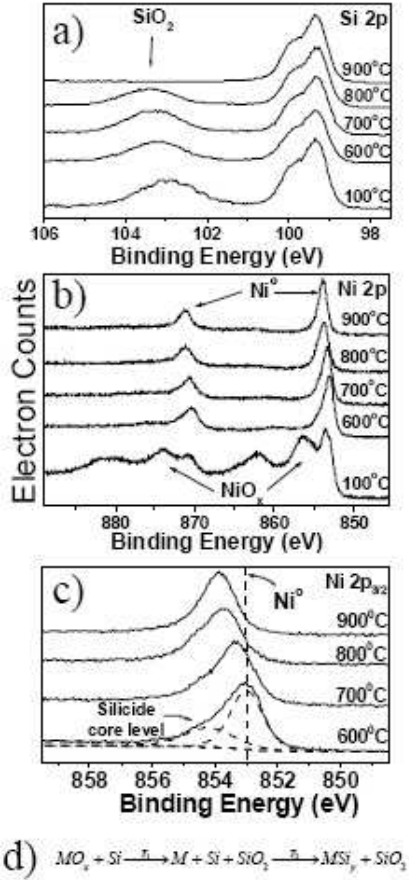


FIG. 3: XPS spectra of a nickel film on clean silicon for the (a) Si 2p and (b) Ni 2p core levels. Similar to the iron catalyst, the nickel is first reduced by through the formation of more silicon dioxide, and then forms a silicide before reaching the single-wall nanotube growth temperature. (c) The nickel silicide begins to form at 600 °C, seen as an up-shift in the Ni 2p core level. By 800 °C, the core level has shifted by 1.0 eV, indicating that all of the nickel has been incorporated into a silicide. (d) Schematic reaction pathway from metal oxide catalyst to the formation of the non-catalytic silicide.

as a high binding energy shoulder on the Ni 2p_{3/2} core level (Figure 3c). As the substrate is further annealed, the Ni 2p_{3/2} level shifts to higher binding energy, reaching a total shift of 1.0 eV by 800 °C where the entire nickel film has been incorporated into the silicide.^[36,37] The chemical progression for both iron and nickel catalyst can be summarized as in Figure 3d. The initial metal or metal oxide is completely reduced by the silicon substrate leading to the growth of a silicon dioxide layer. After being reduced, the metal can then react with the silicon substrate directly, leading to the formation of a silicide.

The initial silicide formation at ~ 600 °C for nickel and ~ 800 °C for iron explains the differing growth yields of single- and multi-walled nanotubes on clean silicon substrates. Since CVD of multi-walled nanotubes on iron occurs at relatively low temperatures, the metal remains unreacted and available for nanotube catalysis. In contrast, the growth of single-walled nanotubes is performed at higher temperatures where all of the catalysts have been consumed by the silicide. In the case of iron presented in Figure 2d, the Fe $2p_{3/2}$ peak is only shifted by 0.2 eV at the multi-walled nanotube growth temperature of 800 °C. This shift is approximately half of the binding energy shift that would correspond to a stoichiometric iron silicide, indicating that catalytic regions of pure iron are still present which permit high yield growth of multi-walled nanotubes. By 900 °C the iron silicide formation is complete, preventing nanotube catalysis and leading to poor growth yield.

Since iron silicide reduces catalytic yield and forms when iron-based catalysts are used on bare silicon wafers but not on highly oxidized wafers, it is important to know how to maintain the iron in a catalytic state without requiring the use of a thick oxide. For electronic applications such as FETs, the use of thinner oxides gives higher gate efficiency due to the increased capacitance of the gate dielectric. de los Arcos and co-authors have shown that iron thin films maintain their catalytic state when they are placed on top of nitrides (TiN) and oxides (Al_2O_3 and TiO_2),^[12,17,38] but the use of silicon oxide would be more compatible with industrial silicon processing. In order to utilize silicon dioxide, it is important to determine what is the minimum thickness required to prevent the formation of a silicide. To determine this, iron catalyst is deposited onto 3, 4, and 8 nm oxides, and we use the measured binding energy of the reduced Fe $2p_{3/2}$ core level around 707.3 eV to detect any silicide formation (Figs. 4a-d). If the silicon dioxide layer is thick enough to prevent silicide formation, the iron core level will remain at 707.3 eV, but if a silicide forms the peak will shift to higher binding energy, where 707.7 eV is the position of the fully formed iron silicide. As seen above for the case of iron or nickel on hydrogen-terminated silicon, as the substrates are annealed some of the iron oxide is reduced by the formation of silicon dioxide, even for iron nitrate on an 8 nm oxide. After this reduction, the metal catalyst could react further with the substrate to form the silicide. For catalyst deposited on the clean silicon (Figure 4a) or a 3 nm oxide (Figure 4b), we see that the iron core level shifts to higher binding energy above 800 °C, indicating the nucleation of the silicide, followed by complete silicide formation at 900 °C. In contrast, heating the catalyst to 900 °C on an 8 nm oxide (Figure 4d) does not lead to

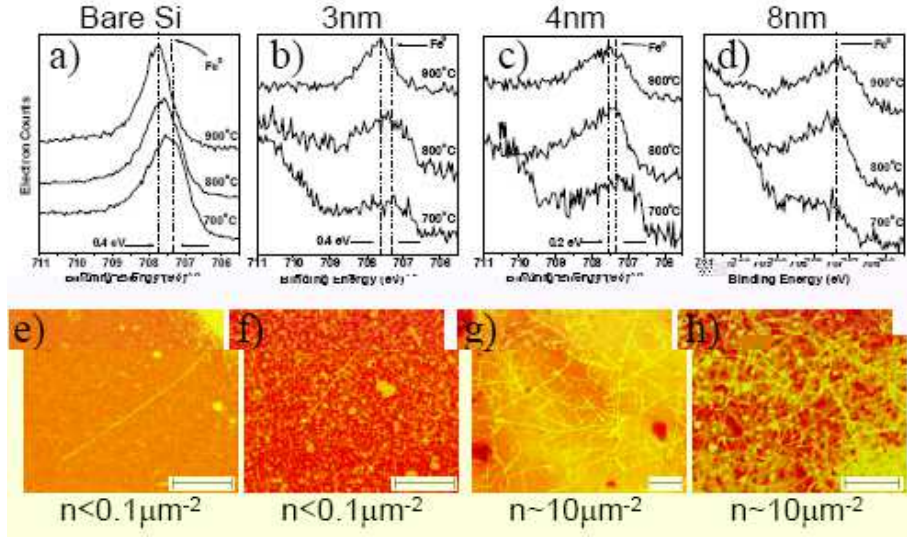


FIG. 4: (a-d) Fe $2p_{3/2}$ core level of iron nitrate on (a) clean silicon, (b) 3 nm SiO_2 , (c) 4 nm SiO_2 , and (d) 8 nm SiO_2 . For clean silicon and a 3 nm oxide layer, silicides form by 900 °C, whereas no silicide is detected for the 8 nm oxide. On a 4 nm oxide, there is a partial shift in the core level, indicating that the catalyst has not been entirely alloyed with the substrate. (e-h) False color SEM images of growths on (e) clean silicon, (f) 3 nm SiO_2 , (g) 4 nm SiO_2 , and (h) 8 nm SiO_2 , showing a reduced yield on clean silicon and 3 nm SiO_2 , but no reduced yield on 4 and 8 nm oxides. All scale bars are 1 μm . Images of growth on clean silicon and 3 nm SiO_2 , (e) and (f), are atypical in that nanotubes are absent on most of the substrates. Images (e) and (f) are presented to show the maximal density of nanotubes grown on each substrate. The density of grown nanotubes is listed beneath each SEM image.

silicide formation. In the case of the 4 nm silicon dioxide layer (Figure 4c), we see a small up-shift of 0.2 eV after the catalyst has been annealed at 900 °C, suggesting that some of the iron has been incorporated into a silicide, but that an appreciable amount of the iron remains in reduced form. Thus, a 4 nm oxide layer represents the minimum thickness that can inhibit the formation of the iron silicide during the growth of single-walled nanotubes at 900 °C. This value is similar to a previous estimate of 5-6 nm, where the role of non-catalytic silicides was conjectured rather than directly shown.^[24]

Having uncovered the minimum barrier oxide thickness in the case of iron catalyst, it is important to determine what mechanism sets this limit. Close observation of the XPS spectra reveals a key signature of the mechanism of the interfacial reaction: the silicide is

forming even though a silicon dioxide layer is present on the surface. This indicates that either the silicon is diffusing up through the oxide to form the silicide, or that the metal is diffusing down. The direction of diffusion is demonstrated most clearly in the case of a nickel thin film on a native oxide substrate (Figure 5). At low temperatures the fully reduced

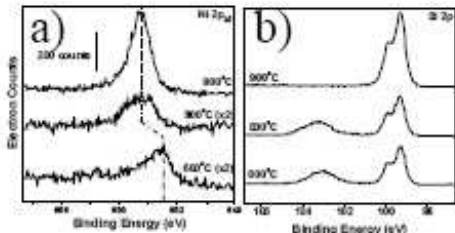


FIG. 5: (a) Ni $2p_{3/2}$ and (b) Si $2p$ core levels for a nickel film catalyst on native oxide. The metallic nickel present at 600 °C has been incorporated into a silicide by 800 °C before the desorption of the SiO_2 layer. When the oxide layer is removed, the nickel signal increases indicating that there is a higher concentration of nickel beneath the oxide than on top due to diffusion of metal through the oxide at lower temperatures.

nickel film coexists with the thin SiO_2 layer, however by 800 °C the Ni $2p_{3/2}$ core level is fully shifted due to the formation of the silicide, while the SiO_2 layer remains. After annealing to 900 °C, to desorb the silicon dioxide layer, the spectra show an increase in intensity from nickel, while the binding energy remains the same. This increase in intensity is clear evidence that the nickel silicide was originally beneath the SiO_2 , where its XPS intensity was reduced due to the finite electron escape depth;^[39] annealing the sample to remove the SiO_2 eliminates the scattering nickel photoelectrons, leading to an increase in the nickel intensity. For the silicide to form beneath the oxide, the metal catalyst must diffuse through the oxide. The diffusion mechanism further explains why single-walled nanotube growth is more inhibited than multi-walled nanotube growth since the diffusion kinetics are enhanced at the higher single-walled nanotube growth temperatures.

Given the diffusion mechanism, one can tailor the oxide thickness to maximize the gate coupling while maintaining the catalyst in an active state. Catalyst diffusion through the oxide is determined by the temperature dependent diffusion constant $D = D_0 e^{-\epsilon/kT}$ and the corresponding diffusion length $\lambda \sim \sqrt{Dt}$, where ϵ is the activation energy for diffusion and t is the diffusion time. Using the bulk diffusion constant for iron in electronic grade

silicon dioxide ($D_o \sim 10^{-4} \text{ cm}^2\text{s}^{-1}$, $\epsilon = 2.8 \text{ eV}$)^[40] one would only expect the iron to diffuse $\sim 1.5 \text{ nm}$ during the temperature ramp to $900 \text{ }^\circ\text{C}$, roughly three times shorter than observed in XPS. The 4 nm diffusion length observed can be explained by a small reduction of $\sim 0.18 \text{ eV}$ in the activation energy, yielding a five-fold increase in the effective diffusion constant. An increased diffusion constant is not surprising for such ultra-thin oxides since they have higher concentrations of pinhole defects as compared to thick oxides. Indeed, previous studies of metals on ultra-thin silicon oxides have shown that pinholes or defects in the oxide significantly enhances the diffusion process.^[40,41,42,43] By determining the critical oxide thickness that prevents silicide formation for iron catalyst, we can extrapolate to determine the critical thickness for cobalt and nickel which are the other common single-walled nanotube catalysts. For cobalt, the bulk diffusion parameters are $D_o \sim 10^{-7} \text{ cm}^2\text{s}^{-1}$ and $\epsilon = 1.7 \text{ eV}$,^[44] leading to a diffusion length and critical oxide thickness of $\sim 12 \text{ nm}$ at a $900 \text{ }^\circ\text{C}$ growth temperature.^[45] This bulk diffusion length is sufficiently thick that high quality oxide layers can be made to prevent defect-enhanced diffusion. For nickel, bulk diffusion ($D_o \sim 1.5 \times 10^{-9} \text{ cm}^2\text{s}^{-1}$, $\epsilon = 1.6 \text{ eV}$)^[46] would predict a $\sim 2.5 \text{ nm}$ critical thickness, which is in the regime of the enhanced diffusion seen for iron. If we assume a proportionate decrease in the activation energy for Ni diffusion (0.1 eV), the critical oxide thickness at the $900 \text{ }^\circ\text{C}$ growth temperature^[47] becomes $\sim 4.1 \text{ nm}$. By minimizing the concentration of defects in the oxide, one could reduce these critical oxide thicknesses further. Though the critical thickness could also be reduced by using a more effective barrier layer than silicon dioxide, the nanotube-gate coupling will also change due to changes in the insulator capacitance.

Having determined the minimum oxide thickness to prevent catalyst diffusion through the oxide layer from XPS, it is important to ensure that the conclusions are consistent with growth observations. Surface reactions observed in UHV may be inhibited when the process is repeated in a CVD reactor where reactant gases can influence catalyst chemistry. Since transition-metal silicides are more stable than transition-metal carbides at nanotube growth temperatures,^[48,49] it is expected that the reactants will not be able to reverse the silicide formation and nanotube catalysis will be inhibited. To test these conclusions, growth was attempted on unannealed pieces of each of the thin oxides. Figures 4e-h show SEM images of the results of this growth test. In the case of growth on hydrogen terminated silicon and 3 nm oxides (Figs. 4e,f), nanotubes are absent on the majority of the substrate. The images

shown depict one of the few locations where nanotubes did grow, and the reported densities represent an upper limit on the nanotube yield. As is readily apparent, there is very little nanotube yield when growth was performed on hydrogen terminated silicon or a 3 nm oxide. In contrast, and consistent with our XPS results, yields on the 4 and 8 nm oxides (figs. 4g,h) are significantly improved.

III. CONCLUSION

In summary, we have used x-ray photoelectron spectroscopy to monitor the formation of silicides that inhibit the growth of carbon nanotubes on silicon. Annealing metal catalysts on hydrogen-terminated silicon or ultra-thin oxide layers leads to the formation of a non-catalytic silicide around 800 °C (Fe) and 600 °C (Ni). By 900 °C, all of the catalyst has been incorporated into the silicide. In order to prevent silicide formation, the oxide substrate must act as an effective barrier to the diffusion of metal catalyst at the high single-walled nanotube growth temperature. In the case of iron, our XPS and growth experiments have shown that oxide layers that are 4 nm or greater are able to inhibit silicide formation at 900 °C, leading to a high nanotube growth yield. By limiting catalyst diffusion through the oxide layer, either with reduced growth temperatures or reduced diffusivity in the oxide, single-walled nanotubes can be grown with high yields on ultra-thin SiO₂ layers.

IV. EXPERIMENTAL

The substrates used in this study consist of highly doped silicon wafers capped with thermally grown SiO₂ (100, 8, 4, or 3 nm), a native (~ 1 nm) oxide, or hydrogen termination. All oxide thicknesses are measured using multi-wavelength ellipsometry and confirmed by direct measurements using atomic force microscopy. The oxide thickness uniformity across the substrates is better than 1 nm. To obtain a clean silicon wafer, a hydrofluoric acid etch is used to remove the native oxide and hydrogen-terminate the silicon. Immediately after hydrogen termination, the catalyst is deposited and the sample is introduced into the vacuum chamber within five minutes in order to limit the formation of a native oxide layer. The quality of the hydrogen termination is confirmed by the low intensity of the oxidized silicon peak in the XPS spectra.

Although there are a large number of catalysts available, many require the incorporation of an insulating matrix, such as alumina, which can influence the chemistry of the catalyst. For example, annealing a thin film of iron on an alumina buffer layer was shown to lead to an oxidation of the iron to Fe_2O_3 .^[17,38] In order to avoid such interactions, we use catalysts that do not require a matrix: iron nitrate and thermally evaporated nickel thin films. The iron nitrate catalyst is prepared by dissolving 50 mg iron (III) nitrate nonahydrate ($\text{Fe}(\text{NO}_3)_3 \cdot 9\text{H}_2\text{O}$) in 100 ml isopropanol and stirring for two minutes.^[50] The substrates are then soaked in the solution for one minute and the sample is dried with flowing nitrogen, forming a thin layer of catalyst over the entire substrate. Nickel catalyst is deposited onto the substrates by electron beam evaporation, resulting in a 7 Å film which decomposes at the growth temperature to form nanoparticles. Chemical vapor deposition tests are performed in an atmospheric pressure reactor. The substrates are brought to the 900 °C growth temperature under argon flow, after which methane (400 sccm) and hydrogen (20 sccm) are used for the 10 minute nanotube growth. The samples are then cooled to room temperature under argon before being removed from the reactor.

XPS is performed in an ion-pumped ultra-high vacuum (UHV) chamber with a working pressure of better than 2×10^{-9} torr, using monochromatic $\text{Al}_{K\alpha}$ (1486.6 eV) x-rays at a resolution of ~ 0.2 eV. Sample heating is performed in UHV by passing current through the silicon substrate and the temperature is measured using an optical pyrometer. After introduction into the UHV chamber, the samples are outgassed at ~ 100 °C for 10 minutes to remove any residual contaminants. In order to mimic the kinetics of the temperature ramp used in a typical CVD growth, the sample is slowly heated from room temperature to the anneal temperature over 5 minutes. After reaching the desired temperature, substrate heating is stopped and the sample is allowed to cool to room temperature. During the anneal, the base pressure in the chamber increases, preventing the acquisition of spectra at the anneal temperature. All energies are corrected to the Si $2p_{3/2}$ core level at 99.3 eV for clean silicon and 103.3 eV for SiO_2 ^[39] to correct for charging effects on the oxide substrates. Quantitative XPS fitting is obtained by fitting raw data to Voigt functions after a Shirley background correction.^[51]

Acknowledgments

The authors acknowledge financial support from the NSF MRSEC program under DMR-0520527, the NSF CAREER program under DMR-0094063, the NSF NSEC program under DMR-0425880, and DMR-0210806.

-
- ¹ R. Saito, G. Dresselhaus, and M. S. Dresselhaus, *Physical Properties of Carbon Nanotubes* (Imperial College Press, London, 1998).
- ² R. Martel, T. Schmidt, H. R. Shea, T. Hertel, and P. Avouris, *Applied Physics Letters* **73**, 2447 (1998).
- ³ S. J. Tans, A. R. M. Verschueren, and C. Dekker, *Nature* **393**, 49 (1998).
- ⁴ S. Chopra, K. McGuire, N. Gothard, A. M. Rao, and A. Pham, *Applied Physics Letters* **83**, 2280 (2003).
- ⁵ J. Kong, N. R. Franklin, C. Zhou, M. G. Chapline, S. Peng, K. Cho, and H. Dai, *Science* **287**, 622 (2000).
- ⁶ C. S. Lee, S. E. Baker, M. S. Marcus, W. Yang, M. A. Eriksson, and R. J. Hamers, *Nano Letters* **4**, 1713 (2004).
- ⁷ H. Dai, J. Kong, C. Zhou, N. Franklin, T. Tombler, A. Cassell, S. Fan, and M. Chapline, *Journal of Physical Chemistry B* **103**, 11246 (1999).
- ⁸ J. Kong, A. M. Cassell, and H. Dai, *Chemical Physics Letters* **292**, 567 (1998).
- ⁹ A. Moisala, A. Nasibulin, and E. I. Kauppinen, *Journal of Physics: Condensed Matter* **15**, S3011 (2003).
- ¹⁰ R. T. K. Baker, J. R. Alonzo, J. A. Dumesic, and D. J. C. Yates, *Journal of Catalysis* **77**, 74 (1982).
- ¹¹ T. de los Arcos, M. G. Garnier, J. W. Seo, P. Oelhafen, V. Thommen, and D. Mathys, *Journal of Physical Chemistry B* **108**, 7728 (2004).
- ¹² T. de los Arcos, F. Vonau, M. G. Garnier, V. Thommen, H.-G. Boyen, P. Oelhafen, M. Duggelin, D. Mathis, and R. Guggenheim, *Applied Physics Letters* **80**, 2383 (2002).
- ¹³ C. Klinke, J. M. Bonard, and K. Kern, *Journal of Physical Chemistry B* **108**, 11357 (2004).
- ¹⁴ Z. Konya, J. Kiss, A. Oszko, A. Siska, and I. Kiricsi, *Physical Chemistry Chemical Physics* **3**, 155 (2001).
- ¹⁵ C. Emmenegger, J. M. Bonard, P. Mauron, P. Sudan, A. Lepora, B. Grobety, A. Zuttel, and L. Schlapbach, *Carbon* **41**, 539 (2003).
- ¹⁶ K. Prabhakaran, Y. Watanabe, Y. Homma, T. Ogino, B. Q. Wei, P. M. Ajayan, K. Shafi, A. Ulman, S. Heun, A. Locatelli, et al., *Langmuir* **19**, 10629 (2003).

- ¹⁷ T. de los Arcos, Z. M. Wu, and P. Oelhafen, *Chemical Physics Letters* **380**, 419 (2003).
- ¹⁸ J. E. Herrera and D. E. Resasco, *Journal of Catalysis* **221**, 354 (2004).
- ¹⁹ K. Nishimura, N. Okazaki, L. J. Pan, and Y. Nakayama, *Japanese Journal of Applied Physics* **43**, L471 (2004).
- ²⁰ B. Yang, M. S. Marcus, D. G. Keppel, P. P. Zhang, Z. W. Li, B. J. Larson, D. E. Savage, J. M. Simmons, O. M. Castellini, M. A. Eriksson, et al., *Applied Physics Letters* **86**, 263107 (2005).
- ²¹ Y. Jung, B. Q. Wei, R. Vajtai, P. M. Ajayan, Y. Homma, K. Prabhakaran, and T. Ogino, *Nano Letters* **3**, 561 (2003).
- ²² F. Maeda, E. Laffosse, Y. Watanabe, S. Suzuki, Y. Homma, M. Suzuki, T. Kitada, T. Ogiwara, A. Tanaka, M. Kimura, et al., *Physica E* **24**, 19 (2004).
- ²³ J. I. Sohn, C. J. Choi, S. Lee, and T. Y. Seong, *Applied Physics Letters* **78**, 3130 (2001).
- ²⁴ A. Cao, P. M. Ajayan, G. Ramanath, R. Baskaran, and K. Turner, *Applied Physics Letters* **84**, 109 (2004).
- ²⁵ C. L. Cheung, J. H. Hafner, and C. M. Lieber, *Proceedings of the National Academy of Sciences* **97**, 3809 (2000).
- ²⁶ D. Kondo, S. Sato, A. Kawabata, and Y. Awano, *Japanese Journal Of Applied Physics* **44**, 5292 (2005).
- ²⁷ W. K. Wong, C. S. Lee, and S. T. Lee, *Journal of Applied Physics* **97**, 084307 (2005).
- ²⁸ N. S. McIntyre and D. G. Zetaruk, *Analytical Chemistry* **49**, 1521 (1977).
- ²⁹ T. C. Lin, G. Seshadri, and J. A. Kelber, *Applied Surface Science* **119**, 83 (1997).
- ³⁰ A. P. Grosvenor, B. A. Kobe, M. C. Biesinger, and N. S. McIntyre, *Surface And Interface Analysis* **36**, 1564 (2004).
- ³¹ M. W. Chase, *Journal of Physical and Chemical Reference Data* p. Monograph 9 (1998).
- ³² B. A. Orlowski, B. J. Kowalski, K. Fronc, R. Zuberek, S. Mickevicius, F. Mirabella, and J. Ghijssen, *Journal of Alloys and Compounds* **362**, 202 (2004).
- ³³ Y. Homma, Y. Kobayashi, T. Ogino, D. Takagi, R. Ito, Y. Jung, and P. Ajayan, *Journal of Physical Chemistry B* **107**, 12161 (2003).
- ³⁴ K. Ruhrschopf, D. Borgmann, and G. Wedler, *Thin Solid Films* **280**, 171 (1996).
- ³⁵ Q. G. Zhu, H. Iwasaki, E. D. Williams, and R. L. Park, *Journal of Applied Physics* **60**, 2629 (1986).
- ³⁶ N. W. Cheung, P. J. Grunthaner, F. J. Grunthaner, J. W. Mayer, and B. M. Ullrich, *Journal*

- of Vacuum Science and Technology **18**, 917 (1981).
- ³⁷ T. T. A. Nguyen and R. Cinti, *Physica Scripta* **T4**, 176 (1983).
- ³⁸ T. de los Arcos, M. G. Garnier, P. Oelhafen, D. Mathys, J. W. Seo, C. Domingo, J. V. Garcia-Ramos, and S. Sanchez-Cortes, *Carbon* **42**, 187 (2004).
- ³⁹ J. F. Moulder, W. F. Stickle, P. E. Sobol, and K. D. Bomben, *Handbook of X-ray Photoelectron Spectroscopy* (Perkin-Elmer, Eden Prairie, MN, 1992).
- ⁴⁰ O. Kononchuk, K. G. Korablev, N. Yarykin, and G. A. Rozgonyi, *Applied Physics Letters* **73**, 1206 (1998).
- ⁴¹ M. Liehr, H. Lefakis, F. K. LeGoues, and G. W. Rubloff, *Physical Review B* **33**, 5517 (1986).
- ⁴² J. T. Mayer, R. F. Lin, and E. Garfunkel, *Surface Science* **265**, 102 (1992).
- ⁴³ E. Conforto and P. E. Schmid, *Philosophical Magazine A* **81**, 61 (2001).
- ⁴⁴ N. A. Fedorovich, *Soviet Physics Solid State* **22**, 1093 (1980).
- ⁴⁵ Y. Ohno, S. Iwatsuki, T. Hiraoka, T. Okazaki, S. Kishimoto, K. Maezawa, H. Shinohara, and T. Mizutani, *Japanese Journal of Applied Physics* **42**, 4116 (2003).
- ⁴⁶ R. N. Ghoshtagore, *Journal of Applied Physics* **40**, 4374 (1969).
- ⁴⁷ L. W. Liu, J. H. Fang, L. Lu, Y. J. Ma, Z. Zhang, H. F. Yang, A. Z. Jin, and C. Z. Gu, *Journal of Physical Chemistry B* **108**, 18460 (2004).
- ⁴⁸ M. Backhaus-Ricoult, *Acta Metallurgica Et Materialia* **40**, S95 (1992).
- ⁴⁹ Y. Pan and J. L. Baptista, *Journal of the American Ceramic Society* **79**, 2017 (1996).
- ⁵⁰ J. H. Hafner, C. L. Cheung, T. H. Oosterkamp, and C. M. Lieber, *Journal of Physical Chemistry B* **105**, 743 (2001).
- ⁵¹ D. A. Shirley, *Physical Review B* **5**, 4709 (1972).